# Viscoelastic Retraction of Single Living Stress Fibers and Its Impact on Cell Shape, Cytoskeletal Organization, and Extracellular Matrix Mechanics

Sanjay Kumar,* Iva Z. Maxwell,† Alexander Heisterkamp,† Thomas R. Polte,* Tanmay P. Lele,* Matthew Salanga,‡ Eric Mazur,† and Donald E. Ingber*

*Vascular Biology Program, Departments of Pathology and Surgery, Children's Hospital and Harvard Medical School, Boston, Massachusetts; †Department of Physics, Division of Engineering and Applied Sciences, Harvard University, Cambridge, Massachusetts; and ‡Mental Retardation Research Center, Children's Hospital, Boston, Massachusetts

ABSTRACT Cells change their form and function by assembling actin stress fibers at their base and exerting traction forces on their extracellular matrix (ECM) adhesions. Individual stress fibers are thought to be actively tensed by the action of actomyosin motors and to function as elastic cables that structurally reinforce the basal portion of the cytoskeleton; however, these principles have not been directly tested in living cells, and their significance for overall cell shape control is poorly understood. Here we combine a laser nanoscissor, traction force microscopy, and fluorescence photobleaching methods to confirm that stress fibers in living cells behave as viscoelastic cables that are tensed through the action of actomyosin motors, to quantify their retraction kinetics in situ, and to explore their contribution to overall mechanical stability of the cell and interconnected ECM. These studies reveal that viscoelastic recoil of individual stress fibers after laser severing is partially slowed by inhibition of Rho-associated kinase and virtually abolished by direct inhibition of myosin light chain kinase. Importantly, cells cultured on stiff ECM substrates can tolerate disruption of multiple stress fibers with negligible overall change in cell shape, whereas disruption of a single stress fiber in cells anchored to compliant ECM substrates compromises the entire cellular force balance, induces cytoskeletal rearrangements, and produces ECM retraction many microns away from the site of incision; this results in large-scale changes of cell shape ($>$ 5% elongation). In addition to revealing fundamental insight into the mechanical properties and cell shape contributions of individual stress fibers and confirming that the ECM is effectively a physical extension of the cell and cytoskeleton, the technologies described here offer a novel approach to spatially map the cytoskeletal mechanics of living cells on the nanoscale.

## INTRODUCTION

Cell shape control is important for regulating mammalian cell growth, differentiation, motility, and apoptosis (1–3) as well as for stem cell fate switching (4). Cells spread when their transmembrane integrin receptors bind extracellular matrix (ECM) proteins; integrins then cluster within focal adhesions, thereby physically anchoring the ECM to the internal actin cytoskeleton (5). Cell shape is modulated by polymerization of actin microfilaments that associate with myosin filaments, and by the resulting actomyosin-dependent traction forces that cells exert on their focal adhesion contacts with the ECM. This process results in assembly of complex cytoskeletal structures composed of long, aligned, actomyosin filament bundles, known as stress fibers, that span between each pair of fixed focal adhesions at the cell base. Because these structures are stiffer than the surrounding cytoplasm (6,7), they provide local shape stability in the sense that their material properties enable them to resist stresses on a short length scale. It remains unclear, however, whether these nanometer-scale actin filament bundles at the cell base contribute to shape stability at the level of the whole cell that can be over a hundred micrometers in length and many micrometers high.

A theoretical model of cell mechanics and recent experimental studies suggest that the level of isometric tension or ''prestress'' in the cytoskeleton may govern cell shape stability (8–12). This model predicts that the stabilizing cytoskeletal prestress is generated both actively by the cell's contractile apparatus through the action of motor proteins, and passively by physical distension of the cell due to its adhesions to a distended ECM, such that the cell, cytoskeleton, and ECM are effectively one prestressed, interconnected structural network (8). Here, basal stress fibers contribute to cell form control by generating tensional forces, transmitting them to the remainder of the entire cytoskeleton and underlying ECM, and bringing these forces into balance. This model, however, remains controversial (13–15), and a major limitation in evaluating it is that it has not been possible to analyze the load-bearing properties of individual stress fibers in living cells.

Although it is clear that stress fibers in cells align and deform in response to external tension fields that are sensed by focal adhesions (16–18), all of the available quantitative data on stress fiber mechanics comes from analysis of stress fibers in vitro, when they are removed from the structural context of the living cell (19,20). It is commonly assumed

*Submitted August 3, 2005, and accepted for publication January 25, 2006.*

Address reprint requests to Donald E. Ingber, MD, PhD, Vascular Biology Program, Children's Hospital, Karp Family Research Laboratories, 11.127 300 Longwood Ave., Boston, MA 02115-5737. Tel.: 617-919-2223; Fax: 617-730-0230; E-mail: donald.ingber@childrens.harvard.edu.

Sanjay Kumar's present address is Dept. of Bioengineering, University of California, Berkeley, California.

Alexander Heisterkamp's present address is Laser Zentrum Hannover, Hannover, D-30419, Germany.



0006-3495/06/05/3762/12 $2.00

doi: 10.1529/biophysj.105.071506

that stress fibers are actively tensed in cells because some actin-binding proteins within the fibers assume a sarcomeric distribution (21,22), and the fibers can be induced to contract in membrane-permeabilized cells by addition of magnesium and ATP (23). Large stress fibers also disassemble in living cells in response to tension dissipation, caused either by inhibiting actomyosin-based contractility or increasing ECM compliance (24–28). However, the pharmacologic tools that are commonly used to isolate contributions of the actin cytoskeleton (e.g., cytochalasin, latrunculin) affect the entire actin lattice that permeates the cytoplasm and underlies the cortical membrane, and thus they do not permit selective interrogation of individual stress fibers. As a result, little is known about the mechanics of single stress fibers in situ, how they contribute to prestress in the cytoskeleton or the surrounding ECM, or their importance for overall shape stability of the whole cell.

The way in which stress fibers bear and distribute loads in their cellular environment has broad implications for models of how cells stabilize their shape. Because actin filaments assemble and disassemble rapidly in lamellipodia and other cellular compartments (29–31), the entire actin cytoskeleton is commonly regarded as highly labile, and cell shape changes are often ascribed to sol-gel transitions driven by changes in actin polymerization (32–34). Indeed, these rapid polymerization dynamics have been invoked to argue that static forces (i.e., tensile prestress) borne by actin-based structures do not contribute significantly to cell shape stability (14). On the other hand, adherent cells have been demonstrated to change their shape from round to fully spread without significantly altering either total microfilament or microtubule mass (35,36). Thus, the relative contributions of actin polymerization-depolymerization dynamics and tensile prestress to cell shape stability remains controversial. Unfortunately, progress in addressing this issue has been limited by a lack of tools capable of disrupting actin structures in living cells without depolymerizing substantial portions of the cytoskeleton.

To tackle these questions directly, we used a femtosecond laser nanoscissor (37,38) to sever individual stress fiber bundles in living cells, while simultaneously visualizing stress fiber retraction, compensatory remodeling of the remaining actin cytoskeleton, and global changes of cell shape. In contrast to past forms of laser surgery used to disrupt actin stress fibers (39,40), this laser uses shorter (femtosecond rather than picosecond) pulses, and thus provides even finer resolution. This newer system can ablate (vaporize) material from regions of $<$300 nm in diameter, with limited damage to surrounding structures as detected by electron microscopy (37) and without compromising cell viability (38). By comparing the observed retraction kinetics produced in response to laser cutting to predictions of mechanical models, we show that individual stress fiber bundles behave like viscoelastic cables. Our studies also reveal that the retraction of individual stress fibers retraction is partially slowed by pharmacological inhibition of Rho-associated kinase (ROCK) and completely eliminated by inhibition of myosin light chain kinase (MLCK), thus demonstrating that the observed retraction behavior is due to the contractile action of unopposed myosin motors. In addition, traction force microscopy using cells cultured on flexible ECM substrates demonstrates that when a single stress fiber is severed, the traction is primarily dissipated into the ECM along its main axis; however, significant traction forces are also released many micrometers from the site of the incision. This reciprocal relationship between single stress fiber tension and ECM traction, and the relevance of this force balance for global cytoskeletal shape stability, is confirmed by the finding that large-scale changes in cell shape and cytoskeletal organization are produced in cells cultured on compliant (soft) substrates, but not on rigid ones, when tensed stress fibers are severed. Taken together, these findings indicate that the ECM is effectively a physical extension of the cell and cytoskeleton, and that the ability of basal actin stress fibers to bear tensile loads is critical for the shape stability of the entire living cell-cytoskeleton-ECM network.

## MATERIALS AND METHODS

### Cell culture

Bovine capillary endothelial cells (passage 10–15) were maintained at 37°C in 10% $CO_2$ on tissue culture dishes in a complete medium composed of low-glucose Dulbecco's modified Eagle's medium (DMEM; Gibco-BRL) supplemented with 10% fetal calf serum (Hyclone, Logan, UT), 10 mM HEPES (JRH-Biosciences, Lenexa, KS), and glutamine (0.292 mg/ml)/penicillin (100 U/ml)/streptomycin (100 g/ml) (Sigma, St. Louis, MO) as previously described (1). For experiments, cells were transfected for 48 h with an adenoviral vector encoding enhanced yellow fluorescent protein (YFP)-tagged G-actin (41), trypsinized (Trypsin–EDTA, Gibco), harvested, and seeded onto glass-bottomed 35 mm dishes (MatTek, Ashland, TX) in complete medium. Before imaging, cells were transferred into a $CO_2$-independent medium (pH 7.3) containing: $CaCl_2$ (1.26 mM), $MgSO_4$ (0.81 mM), KCl (5.36 mM), $KH_2PO_4$ (0.44 mM), NaCl (137 mM), $Na_2HPO_4$ (0.34 mM), D-glucose (5.55 mM), L-glutamine (2 mM), sodium pyruvate (1 mM), HEPES (20 mM) pH 7.4, 1% bovine serum albumin, 10% calf serum, and MEM essential and nonessential amino acids (Sigma) (42). For ROCK inhibition studies, cells were treated with Y27632 (Calbiochem, San Diego, CA) for 1 h at 10 $\mu$M. For MLCK inhibition studies, cells were treated with ML7 (Sigma) for 30 min at 67 $\mu$M.

### Laser nanoscissor and photobleaching

For measurements of retraction kinetics of stress fibers, we used a previously described custom-built laser nanoscissor system that ablates material at the laser focus based on multiphoton absorption (37,38). Briefly, a passively mode-locked oscillator delivers 100-fs laser pulses at a repetition rate of 80 MHz and a central wavelength of 790 nm. These pulses are amplified in a chirped-pulse system to energies of up to 1 mJ at a reduced repetition rate of 1 kHz and then attenuated to energies known to produce subcellular material ablation at sub-300 nm precision (1–2 nJ). The laser light is then focused onto the intracellular target with a 63×, 1.4-NA oil immersion objective lens (Zeiss Plan-Apochromat, Thornwood, NY) that is also used for real-time imaging. The sample is epi-illuminated with light from an ultraviolet lamp that passes through the appropriate filter cube; fluorescence emission is collected through the objective lens and recorded by a camera (Photometrics

CoolSNAP*cf*, Tucson, AZ). Images were collected using IPLab (Scanalytics, Rockville, MD).

For studies in which the nanoscissor was combined with either photobleaching or traction force microscopy, we used a Zeiss upright laser scanning confocal microscope (LSM 510 Meta/NLO) equipped with a 63×, 0.9-NA water-dipping objective optimized for infrared imaging (Zeiss IR-Achroplan). To visualize YFP-actin and Texas red-labeled microspheres, we scanned the sample with the 488-nm laser line attenuated to 10% maximum transmission. Both YFP and Texas red emission were collected through the objective lens and then separated using primary and secondary dichroic beam splitters. Bandpass filters appropriate for either Texas Red or YFP emission fluorescence positioned in front of separate photomultiplier tubes enabled simultaneous red and green imaging. Single stress fiber incision with the nanoscissor was accomplished by focusing energy from a pulsed Ti:Sapphire laser at 100% transmission (Chameleon, Coherent, Santa Clara, CA) over a 0.5-$\mu m^2$ area within the body of the stress fiber for 15 iterations (~170 $\mu$s) through the objective lens at a wavelength of 740 nm, nominal laser-head power of 1.5 W, pulse duration of 140 fs, and repetition rate of 90 MHz. For photobleaching, fluorescent structures were irradiated with a 488-nm laser for 150 iterations at 100% transmission. Images were collected using the Zeiss LSM 510 software (version 3.2). All experiments on both microscopes were performed at 37°C using a temperature-controlled stage. In both cases, the objective lens of the microscope was focused on the plane directly above and adjacent to the cell base to ensure interrogation of basal stress fibers.

## Traction force microscopy

Fibronectin-coated polyacrylamide substrates for traction force microscopy (Young's modulus of ~3.75 kPa) were prepared on glass coverslips, as previously described (43,44). Texas red-labeled microspheres (0.5 $\mu$m diameter, Molecular Probes, Eugene, OR) were suspended in the polyacrylamide before gel formation and used as fiduciary markers. Maps of substrate displacement (strain) and traction relaxation associated with single stress fibers were computed from bead positions before and after stress fiber incision using Fourier transform traction cytometry (45). To measure tractional force returned to the ECM substrate by the cell (i.e., traction relaxed), we used the positions of the fiduciary markers before laser incision as the baseline state, rather than the positions of the beads in the unstressed (cell-free) gel. Cells were cultured and imaged on these substrates under the conditions described above. Changes in cell shape induced by laser severing of individual stress fibers were measured by using computerized image analysis (Zeiss LSM 5 Image Browser) to quantify alterations in the longest cell diameter oriented parallel to the severed fiber. In all cases, these length measurements were made at the focal plane of stress fiber incision, near the cell-ECM interface. The contrast of fluorescent images of cells expressing YFP-actin was digitally enhanced to visualize the thinnest portions of the cytoplasm, and thereby optimally define the cell periphery in these studies. The Student's *t*-test was used to determine statistical significance between changes in cell length induced by stress fiber cutting in cells cultured on rigid versus compliant ECMs.

# RESULTS

## Disruption of individual actin stress fibers in living cells

To directly probe the mechanical properties of actin filament bundles in situ, we used a femtosecond laser nanoscissor (37,38) to physically sever single stress fibers in cultured endothelial cells that expressed YFP-actin. YFP-actin distributed in a stress fiber-like pattern (Fig. 1 *A*) identical to that displayed by endogenous actin in these cells (41); the transfected cells also attached, spread, moved, and proliferated normally. When femtosecond laser pulses were applied

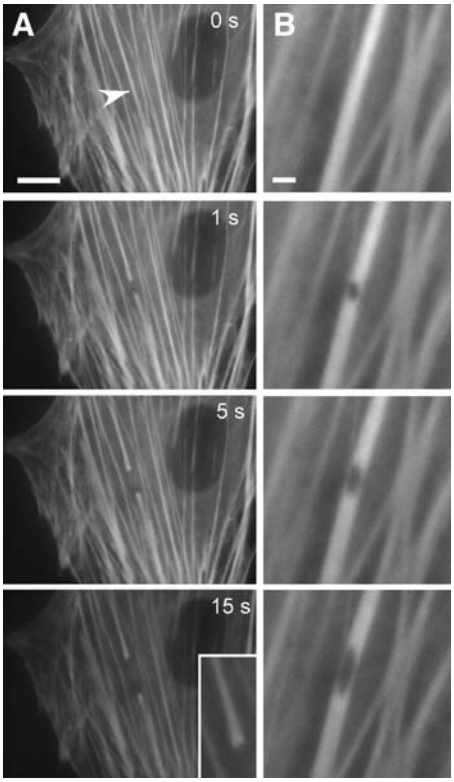


FIGURE 1 Incision of stress fibers in living cells using a laser nanoscissor. (*A*) Severing and retraction of a single stress fiber bundle in an endothelial cell expressing EYFP-actin. As the stress fiber retracted over a period of 15 s, the severed ends splayed apart (*inset*). (Arrowhead indicates the position of the laser spot; bar = 10 $\mu$m) (*B*) Strain relaxation of a single stress fiber bundle after a 300-nm hole was punched in the fiber using the laser nanoscissor. The hole became elliptical as it distended along the tension field line. (Bar = 2 $\mu$m)

to the central region of a single stress fiber within living cells cultured on rigid fibronectin-coated glass cover slips, the severed ends immediately (<1 s) retracted and progressively pulled farther apart over a course of ~15 s, reflecting a release of isometric tension (Fig. 1 *A*). The newly severed ends also ''frayed'' or widened (Fig. 1, *inset*), as expected for a stretched elastic element that is suddenly unloaded (46). When the laser was focused on a circular area smaller than the width of a single stress fiber (<300 nm diameter), a small puncture wound was created without completely severing the fiber (Fig. 1 *B*). This hole progressively elongated along the main axis of the fiber over a course of seconds, illustrating the rearrangement of strain as the stress fiber attempted to accommodate the loss of tensile strength while supporting the same load; in some cases, complete tearing of the fiber was observed after 10–20 s (not shown).

Because previous efforts to sever cytoskeletal elements with picosecond laser pulses produced rapid filament depolymerization (47), we needed to verify that the shortening of the severed ends was due to physical retraction, rather than progressive material loss. To distinguish between these possibilities, we severed stress fiber bundles immediately

adjacent to bifurcation points. If the stress fiber retraction we observed is due to rapid release of actin monomers over the time scale of the experiment, then the branch point should be lost as the severed ends depolymerize; conversely, if the severed ends retract, then the branched end should pull back as an intact structure (Fig. 2 *A*). When we irradiated stress fiber bundles at these branched locations, we observed that the branched end retracted and deformed as an intact structure and remained so for more than 3 min after incision (Fig. 2 *B*). This finding confirms that stress fiber irradiation does not induce substantial actin depolymerization on the time scale of this experiment.

Additional evidence that nanoscissor irradiation resulted in physical retraction of the cut ends of the stress fiber, rather than wholesale disassembly, came from experiments in which we combined the laser nanoscissor method with laser photobleaching. Photobleaching does not sever stress fibers; instead, it selectively renders portions of these cytoskeletal structures optically invisible which may then be used as fiduciary marks to track movements of individual stress fibers (48–50). We photobleached a line across several parallel stress fibers in a living cell by irradiating them with 488-nm laser light at high intensity; the bleached regions remained stable over a time scale of minutes, with minimal fluorescence recovery ((49) and our unpublished observations). When the nanoscissor was then used to sever one of these stress fibers at a point distant from the photobleached region, we observed that the bleached portion of that fiber displaced more than a micrometer away from the incision site causing it to move out of alignment with the bleached portion of the adjacent fibers (Fig. 2 *C*, Supplemental Movies 1 and 2). This result clearly demonstrates that the stress fiber physically retracts throughout its length when it is dissected; disassembly would result in shortening of the severed ends without translation of the bleached zone.

## The mechanical properties of a single living stress fiber

From the dynamics of the fiber retraction, we directly determined the viscoelastic properties of a single stress fiber in its normal physiological context within a living cell. The length of the gap between the retracting ends of the incised fiber increased with kinetics described by a single time constant and asymptotically approached a value equal to the distance between the unstressed (resting) severed ends (Fig. 3 *A*). This trajectory matched that predicted for damped recoil of an elastic fiber, i.e., a viscoelastic cable ($L = L_o(1 - \exp(-t/\tau)) + D_a$) (51,52), represented schematically as a spring and dashpot in parallel (Fig. 3 *A*, *inset*). In this model, $L$ is the distance retracted (one-half the distance between the severed ends), $L_o$ is the asymptotic value of that distance, $t$ is time after severing, $\tau$ is a characteristic time constant equal to the ratio of the material's damping coefficient to its Young's modulus, and $D_a$ is the length of stress fiber immediately destroyed by the laser upon irradiation (37). The damping coefficient arises from a combination of the intrinsic viscoelasticity of the stress fiber and that of the surrounding medium.

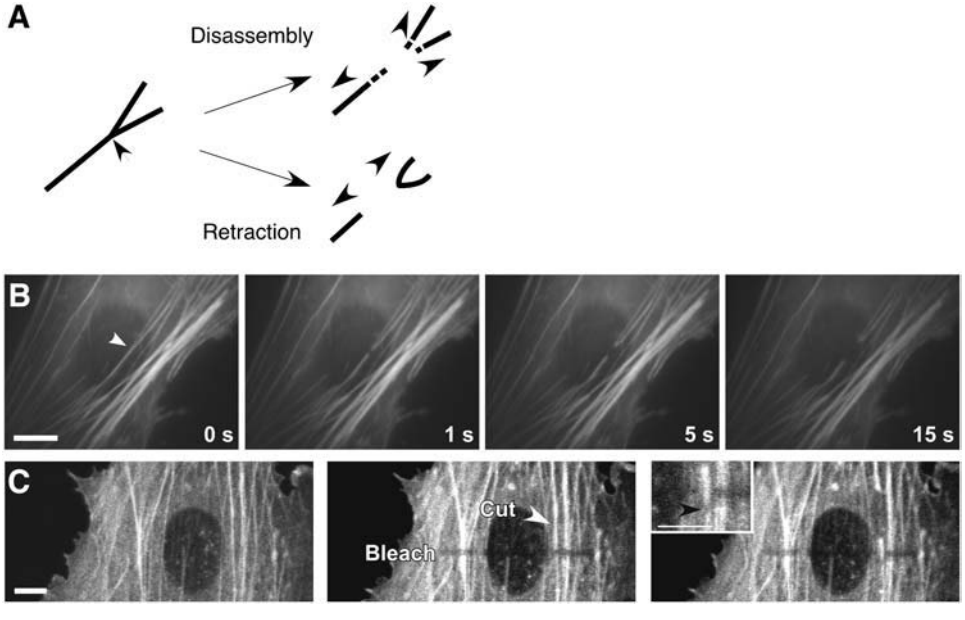


FIGURE 2 Stress fibers retract rather than disassemble after incision. (*A*) Schematic of predicted observations in the case of stress fiber retraction versus disassembly in response to laser incision. In the case of actin depolymerization (*top*), both severed ends of the bundle should disassemble, including the branch point. In the case of passive elastic retraction (*bottom*), the branched portion of the bifurcation will remain whole after irradiation and physically retract as an intact structure. (*B*) Laser irradiation of a stress fiber bundle near a bifurcation and retraction of an intact stress fiber bundle fork in a living cell. (Arrowhead, laser position; bar = 10 $\mu$m) (*C*) Stress fiber retraction monitored by motions of photobleached regions. An optical fiduciary line was written across many parallel EYFP-containing stress fibers by photobleaching them, hence making these regions optically invisible without damaging them. When one of these stress fibers was cut the bleached portion of this fiber translated in the direction of retraction (downward in this view) relative to the other neighboring fibers (white arrowhead indicates laser spot position; black arrowhead in Inset shown at higher magnification indicates movement of the bleached region of the cut stress fiber relative to the neighboring fibers). (Bar = 10 $\mu$m). (See also Supplemental Movies 1 and 2.)

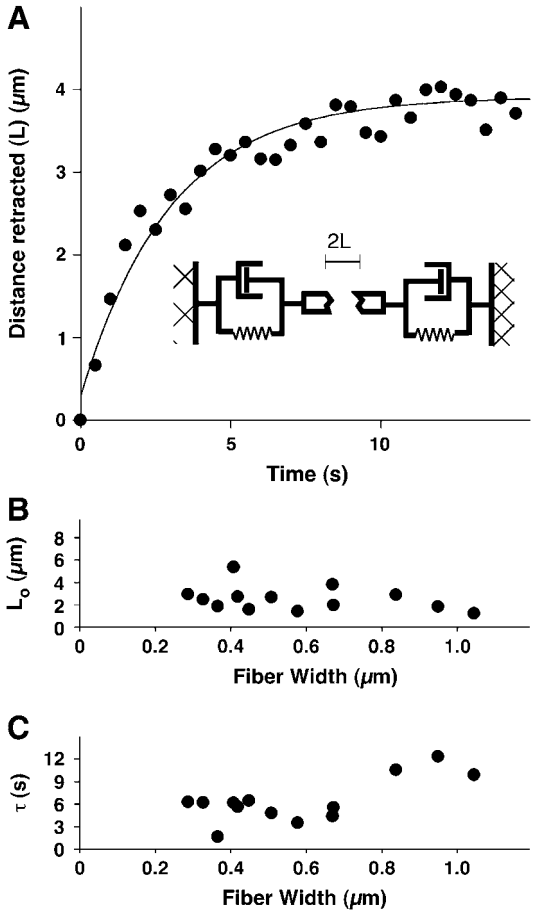


FIGURE 3 Kinetics and nanomechanical modeling of stress fiber retraction. (*A*) Time course of fiber retraction, where retraction distance is defined as one-half the distance between the severed ends of the stress fiber. The line corresponds to the predicted retraction of an elastic and viscous element in parallel: $L = D_a + L_o(1 - \exp(t/\tau))$, where $L$ is the retraction distance, $L_o$ is the maximum retraction, $t$ is time, $\tau$ is the ratio of the drag coefficient to the Young's modulus, and $D_a$ is the material loss due to ablation. (*B*) Effect of stress fiber bundle width on $L_o$. (*C*) Effect of stress fiber bundle width on $\tau$. The data in panels *B* and *C* were obtained by severing one stress fiber per cell in 13 different cells (SEM was less than 10% of the mean).

An important feature of this simple model is that $L_o$ and $\tau$ do not depend explicitly on fiber width. Consistent with these predictions, the experimental data confirmed that there was no clear correlation between either of these mechanical parameters and apparent fiber width for fibers between 0.2 and 0.8 $\mu$m wide (Fig. 3, *B* and *C*). At widths greater than 0.8 $\mu$m, $\tau$ rose significantly ($p < 0.001$) suggesting that stress fibers of this size were effectively less elastic and/or more viscous.

Interestingly, material loss from the stress fiber could also conceivably follow first-order unbinding kinetics and therefore explain the observed retraction data. Indeed, even though each stress fiber normally bears significant tensional loads and therefore functions as a static cable, the individual actin-based subunits contained within the intact filaments continuously turn over. To visualize this in our system, we conducted fluorescence recovery after photobleaching (FRAP) measurements on these stress fibers and found that the half-time for fluorescence recovery for actin was ~5 min. This timescale of molecular turnover matches that found in previous FRAP studies of actin in stress fibers in fibroblasts (48). Most importantly, it did not change significantly after the fiber was severed and tension was dissipated, showing that stress fiber tension does not significantly alter actin subunit binding kinetics under these experimental conditions. This finding, together with the branch retraction and photobleaching studies, make it exceedingly unlikely that the observed stress fiber retraction is due to actin depolymerization.

## Tensional prestress in stress fiber bundles

Although past studies have suggested that actomyosin filament bundles can actively generate contractile forces through the action of myosin motors, this functionality has never been demonstrated directly within individual stress fibers in living non-muscle cells. To experimentally probe stress fiber contractility, we inhibited MLC phosphorylation, which is required for myosin motor activity, with two pharmacological agents that work by distinct mechanisms. First, we used the ROCK inhibitor Y27632 (53) at a dose (10 $\mu$M) that has been shown to optimally dissipate cytoskeletal tension and maximally inhibit a wide variety of tension-dependent behaviors in cultured cells, including endothelial cells (54–56). As expected, inhibition of active tension generation dramatically reduced both the initial rate and final degree of retraction measured over a period of 15 s (Fig. 4). Isolated stress fibers treated with Mg-ATP similarly contract with a smaller amplitude and velocity in the presence of MLCK inhibitors in vitro (19); however, Y27632 only inhibits one of many signaling pathways responsible for activation of MLC phosphorylation and tension generation.

To more directly inhibit stress fiber contraction, we next treated cells with the MLCK inhibitor, ML7 (57). Stress fiber incision after direct inhibition of MLCK resulted in a minimal retraction of ~400 nm, of which at least 150 nm can be accounted for by material destruction by the laser (approximately half the diameter of the puncture wound in Fig. 1 *B*). Presumably, any additional retraction that did occur is due to a small amount of MLCK-independent motor activity or to passive relaxation of the stretched stress fiber. Taken together, these data strongly suggest that stress fiber elasticity in untreated cells is primarily due to MLCK-dependent myosin contraction and that stress fibers are tensionally prestressed in a predominantly active fashion within living cells.

## Contributions of a single stress fiber to ECM mechanics and cell shape control

The finding that the viscoelastic properties of individual stress fibers depend on the presence of contractile elements is

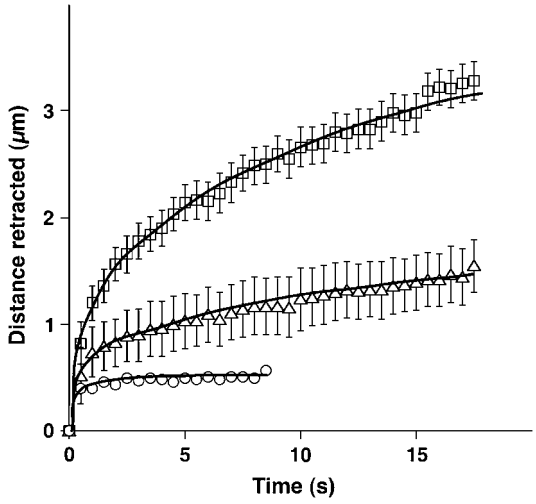


FIGURE 4 Contributions of active contraction versus passive prestress to stress fiber mechanics. Stress fiber bundles were incised in untreated control cells (*squares*, $N = 13$), cells treated with the ROCK inhibitor Y27632 (10 $\mu$M) for 1 h (*triangles*, $N = 19$), and cells treated with the MLCK inhibitor ML7 (67 $\mu$M) for 30 min (*circles*, $N = 16$). Error bars represent mean $\pm$ SE; solid lines are only visual guides. In all cases, one to two stress fibers were severed per cell in multiple cells.

consistent with the broader notion that tensile forces borne by stress fibers underlie the cell's ability to exert traction on the ECM, and to establish a mechanical force balance between the cell and the ECM. In studies of cells attached to rigid ECM-coated glass substrates, however, incision of a single stress fiber failed to produce any apparent change in neighboring stress fibers or in the overall shape of the cell (as measured by its projected ''footprint'' on the substrate) over the course of several minutes (Fig. 1 *A*). Even when several large, parallel stress fibers were successively severed, cell shape remained remarkably stable, even after several minutes (Supplemental Movie 3). However, any transfer of force from the actin stress fibers to the ECM may be hidden due to the rigidity of the glass culture substrate that can bear mechanical loads much greater than those exerted by the entire cell. This is important because the ECM in living tissues is much more compliant than glass, and cells often exhibit more physiologically relevant functions when cultured on flexible substrates (28,58,59). To directly measure the contribution of a single stress fiber to cell traction, we therefore severed individual stress fibers within cells cultured on flexible, fibronectin-coated polyacrylamide gels containing nanometer-sized fluorescent beads while simultaneously performing traction force microscopy (43,45,60). We then calculated traction forces released by the cells and transferred to the ECM from the measured bead displacements and the known Young's modulus (3.75 kPa) of the gel as previously described (44,45).

Laser incision of a single stress fiber bundle released isometric tensional forces previously borne by the cytoskeleton, and produced compensatory relaxation of the ECM substrate which was already tensed (prestressed) because of the tractional forces exerted by the adherent cells. Disruption of the cytoskeleton-ECM force balance by laser ablation of a single stress fiber resulted in ECM relaxation as visualized by outward movement of the beads embedded in the flexible ECM gel (Fig. 5 *A*; also see Supplemental Movie 4). Traction force microscopic analysis revealed that the greatest bead displacements (Fig. 5 *B*) and ECM retraction forces (Fig. 5 *C*) primarily oriented along the main axis of the cut stress fiber in this cell. These stresses initially concentrated within localized sites near the ends of the cut stress fiber, presumably where they insert on focal adhesions, but then progressively transferred to multiple other locations throughout the cell over time (Fig. 5 *C*).

Similar analysis of multiple cells revealed that laser ablation of a single stress fiber and associated disruption of the cellular force balance resulted in rapid, increase in the force transferred to the ECM that reached a plateau value of $\sim$179.5 Pa within $\sim$30–40 s (Fig. 6 *A*). Because bead displacements were measured relative to the initial bead positions (i.e., when cells had already been allowed to spread and tensionally prestress the flexible ECM) and we do not know the strain distribution of the unstressed gel, we cannot determine the total prestress borne by these cells. However, when we cultured endothelial cells on similar polyacrylamide gels and measured bead positions before and after the cells were chemically detached from their adhesions, the average whole-cell traction was determined to be 307 $\pm$ 55 Pa, a value similar to that exhibited by the same cells in a past study (61). Thus, the incision of one stress fiber dissipated a significant portion (>50%) of the total prestress within these cells within 30 s after cutting, when attached to a flexible ECM substrate.

Importantly, this shift of forces from the actin cytoskeleton to the flexible prestressed ECM also resulted in large-scale structural rearrangements in the remaining actin cytoskeleton as well as global changes of cell shape. A comparison of fluorescence images of cells before and after laser ablation clearly demonstrates that although cutting a single stress fiber produced only local fiber retraction of that fiber at the point of laser cutting and no changes in cell form in cells on rigid dishes (Figs. 6 *B* and 7 *A*), similar ablation of a stress fiber in cells on flexible substrates resulted in both this local effect and global rearrangements of multiple other stress fibers distributed throughout the whole length of the cell (Fig. 7 *B*). Again the largest outward displacements occurred along the main axis of the cut fiber (Fig. 7 *B*), and this corresponded to regions of the underlying ECM that exhibited the greatest lateral displacements (Fig. 7 *C*) and relaxation forces (Fig. 7 *D*). Even when most stress fibers were oriented in parallel to the one cut by the laser (as shown in Fig. 5), the remaining fibers located throughout the cytoplasm extended and thinned as the released tension was shifted from the cut fiber to these remaining cytoskeletal elements and their linked ECM adhesions (Supplemental

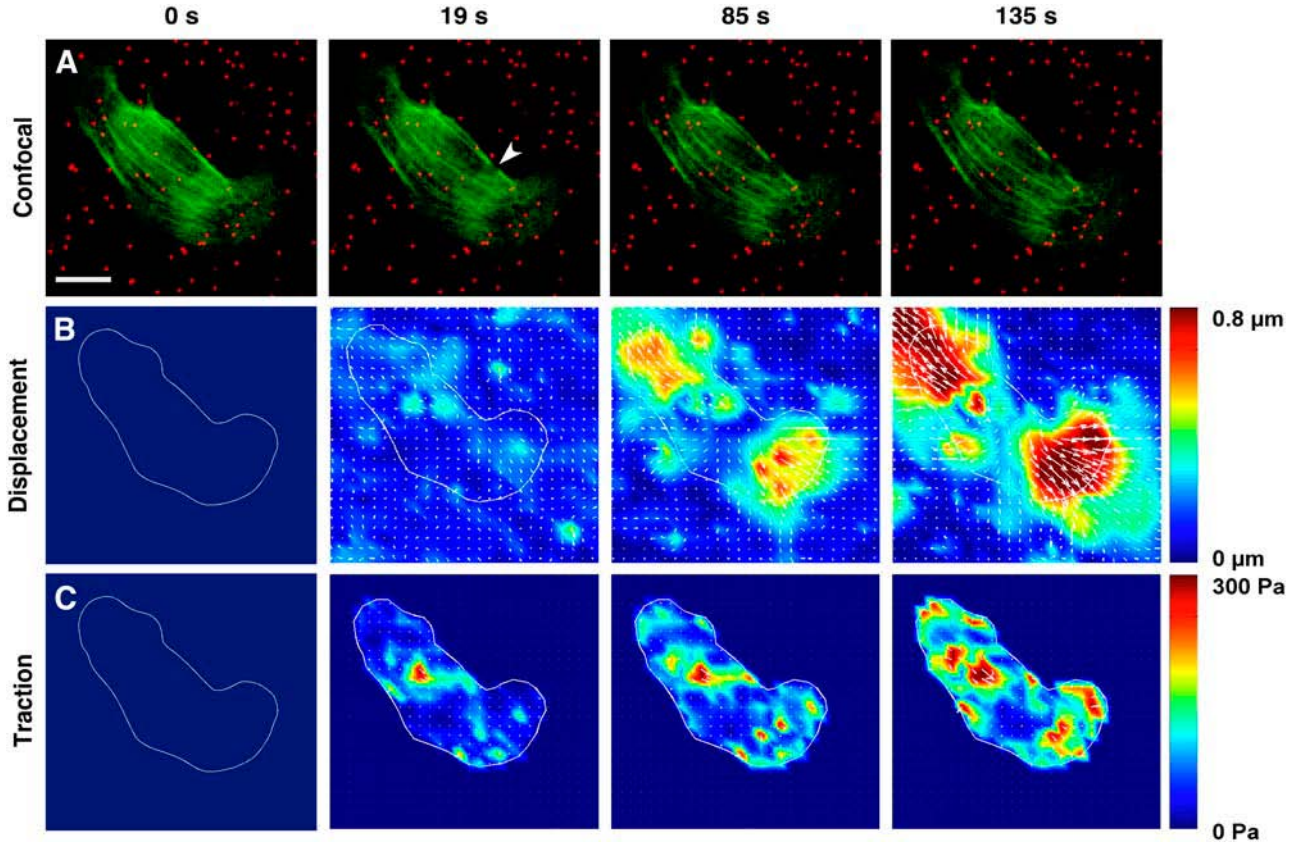


FIGURE 5 Contribution of a single stress fiber to cell traction forces and ECM mechanics visualized over time using traction force microscopy. Endothelial cells were transfected with YFP-actin and cultured on flexible fibronectin-coated polyacrylamide substrates containing embedded fluorescent nanobeads. A stress fiber was then irradiated and severed, and substrate stress and strain maps were calculated from the resulting bead displacements. (*A*) Spatial rearrangements of the actin cytoskeleton (*green*) and embedded beads (*red*). (Arrowhead indicates point of laser ablation; Bar = 20 $\mu$m). (These spatial changes are most clear in Supplemental Movie 4.) (*B*) Changes in bead displacements and ECM substrate strain distribution. (*C*) Changes in cell traction forces relaxed into the ECM substrate. Maps of substrate displacement (strain) and traction associated with single stress fibers were computed from bead positions before and after stress fiber incision.

Movie 4). By measuring the maximum length of the cell at the focal plane of laser ablation and along the axis of the severed stress fiber, we were able to quantify cell shape before and after stress fiber incision. This morphometric analysis revealed that the nanometer-sized incision of a single stress fiber resulted in nearly a 6% increase in cell length on flexible substrates, whereas there was no significant change in length in cells on rigid glass substrates (Fig. 6 *B*). Thus, alterations in the cellular force balance due to dissipation of tensile prestress within a single stress fiber located close to the basal surface of the cell resulted in structural rearrangements and changes in form throughout the entire cytoskeleton, as well as within its underlying ECM. These results confirm that the ECM is a physical

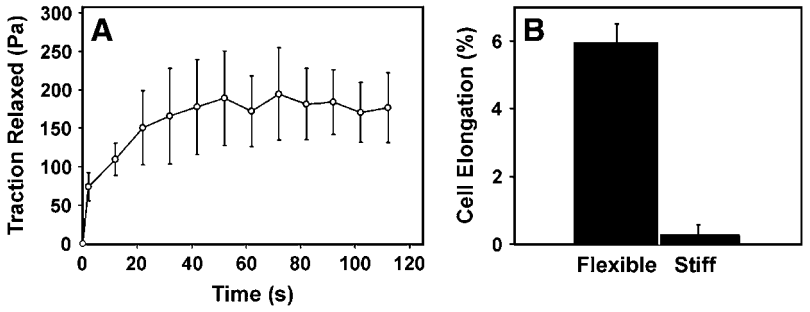


FIGURE 6 Effect of cutting a single stress fiber on force transfer to the ECM and associated changes in cell shape. (*A*) Graph showing changes of cell traction forces relaxed into the ECM substrate measured over time after laser ablation of a single stress fiber using traction force microscopy ($N = 5$; data are presented as mean ± SE). (*B*) Quantification of the effect of stress fiber incision on the global shape of cells adherent to flexible versus rigid ECM substrates. The bar graph depicts the fractional increase in cell length along the main axis of the cut stress fiber and demonstrates a significant increase in cell strain only within cells on flexible substrates ($N > 8$ cells for both substrates; $p < 0.000001$; similar results were obtained in two separate sets of experiments).

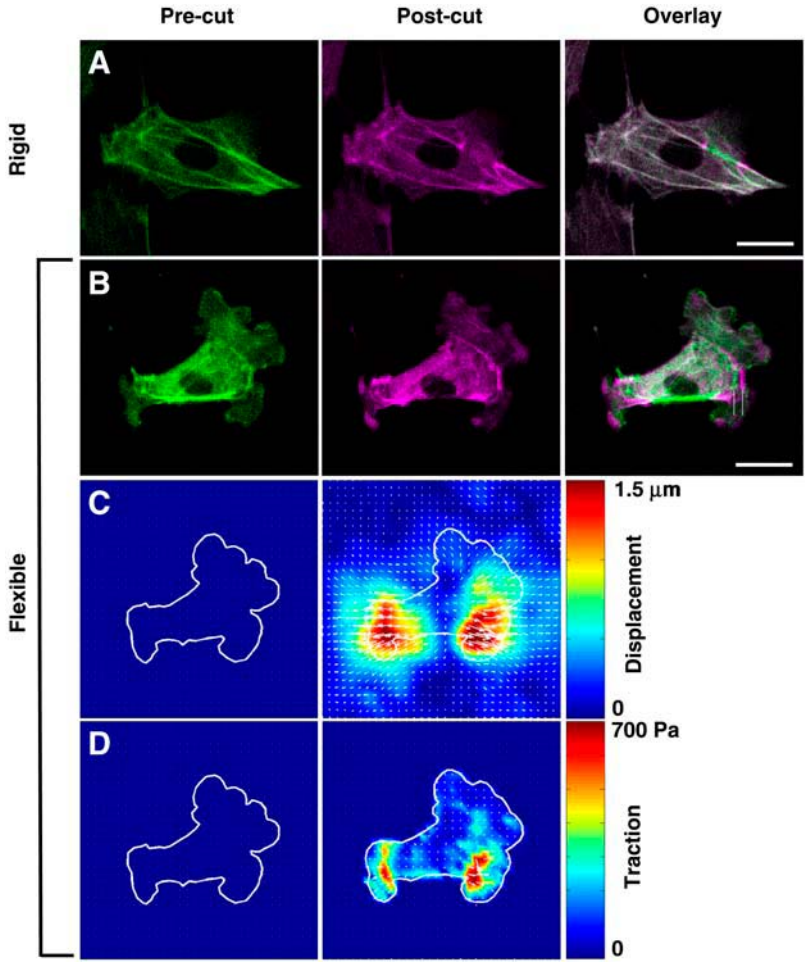


FIGURE 7 Fluorescence microscopic (*A*, *B*) and traction force microscopic (*C*, *D*) images showing the effects of stress fiber incision on cytoskeletal organization, global cell shape and ECM mechanics. A single stress fiber was incised in a cell cultured on either rigid glass (*A*) or a flexible polyacrylamide ECM substrate (*B–D*; stiffness = 3.75 kPa). (*A*, *B*) The actin cytoskeleton is depicted in green before incision (Pre-cut, *left column*) and magenta after incision (Post-cut, *middle column*); when the two images are overlaid (Overlay, *right column*), cytoskeletal regions which did not change position appear white, whereas those that rearranged retain their distinct green and magenta colors. Note that stress fiber incision resulted in global cytoskeletal rearrangements only in the cell on the flexible substrate (*B*), including wholesale outward translation of the whole cell and cytoskeleton along the main axis of the cut fiber. The two vertical white lines indicate a vertically oriented stress fiber located many micrometers away from the site of incision in the right portion of the cytoskeleton that undergoes large-scale lateral displacement in response to stress fiber ablation (Bar = 10 $\mu$m). (*C*) Change in bead displacements and ECM substrate strain distribution. (*D*) Change in cell traction forces relaxed into the ECM substrate.

extension of the cell and cytoskeleton, and that cell shape stability requires maintenance of isometric tension within the entire cytoskeleton, not just in stress fibers at the cell base (8).

## DISCUSSION

We used a femtosecond laser nanoscissor to sever individual stress fibers in living cells, quantified their retraction kinetics, probed biochemical contributions to their elasticity, and examined their contributions to the overall shape of cells cultured on rigid versus compliant ECM substrates. These data demonstrate that stress fiber bundles behave as viscoelastic cables, a concept that has been widely assumed but never directly experimentally demonstrated in living cells. Similar systems that utilized ultrashort lasers pulses have been previously used to sever microtubules (47), mitotic spindles (62,63), mitochondria (38,64), and chloroplasts (65) in living cells. In particular, stress fiber bundles have been irradiated and severed with picosecond lasers in the past (39,40), but with insufficient spatial or temporal resolution to quantify retraction dynamics, or the transfer of strain to the ECM. By carefully tracking the retraction of severed stress fibers while manipulating intracellular tension and ECM compliance, we were able to characterize the mechanical properties of individual stress fibers and define their contribution to the shape stability system of the entire cell with unprecedented precision.

The fact that we observed this behavior in living cells is critical, because previous in vitro work with single actin filaments (66–69), reconstituted actin gels (70), and isolated myofibrils (71,72) has produced equivocal descriptions of stress fiber mechanics. For example, stress fibers have been widely described as either tensile (73), elastic (74), or viscoelastic (75). Our work represents the first unequivocal demonstration that stress fiber bundles retract viscoelastically within the complex living cytoplasm. These findings also confirm that individual stress fibers are tensed almost entirely by actomyosin motors, as evidenced by the complete abrogation of stress fiber retraction when MLCK is inhibited. The dose of Y27632 used in this study has been shown to profoundly (and optimally) alter cell shape and cytoskeletal morphology (54), whole cell prestress (56), cell migration speed (55), and focal adhesion size and turnover (76) in multiple cell types, including endothelial cells (76). Thus, the incomplete inhibition of stress fiber retraction by Y27632

reported here is probably not due to a failure of the cells to optimally respond to the treatment. Instead, the differential effects of Y27632 (ROCK inhibitor) and ML7 (MLCK inhibitor) on stress fiber retraction likely reflect the different mechanisms through which stress fiber myosin activity is regulated. MLCK facilitates myosin activity—and therefore stress fiber contractility—by phosphorylating MLC, whereas ROCK accomplishes this primarily by inhibiting MLC phosphatase, although it also may phosphorylate MLC directly (77–79). The factors that determine the relative contributions of these two pathways to myosin activity are poorly understood, and it has recently been proposed that these pathways are spatially regulated as well (i.e., the contractility of fibers at different locations in the same cell may be under the influence of either MLCK or ROCK; (80,81)). Rho has also recently been implicated in directing the orientation of stress fibers in response to ECM stretch (82). Our finding that ML7 inhibits stress fiber retraction much more completely than Y27632 suggests that for the subset of stress fibers considered here, prestress is chiefly determined by MLCK, not ROCK. The myosin-dependence of stress fiber retraction implies that the prestress borne by these structures is due much more to active tension generation by myosin than to simple passive distortion (stretch) between points of attachment to the ECM (i.e., focal adhesions), at least in cells cultured on rigid glass dishes. In other words, prestress is actively generated internally by actomyosin filament sliding within the stress fiber.

Recently, elasticity measurements have been reported for stress fibers isolated from smooth muscle cells (20). Here, stress fibers shortened ~15% within 1 s of being mechanically dislodged from rigid ECM substrates, thereby leading to the conclusion that stress fibers in these cells are passively strained ~20% of their unstressed length. These measurements are complicated, however, because they were carried out after cell lysis, chemical digestion of the surrounding cytoskeleton, and mechanical disruption of focal adhesions. In a living cell, these supporting elements would all serve to brace a retracting stress fiber after incision, and our failure to observe substantial passive retraction in living cells reinforces the notion that stress fibers are intimately connected to surrounding structural networks, both inside and outside of the cell. Our findings therefore provide additional evidence for the need to carry out micromechanical analysis of cytoskeletal elements in the physical context of living cells.

Although stress fibers behave as viscoelastic cables for a large range of fiber widths, the thickest stress fibers deviate from this behavior and retract with greater effective drag. These larger fibers may either represent a distinct population of structures with unique load-bearing or contractile properties, or they may have more connections with the surrounding cytoskeleton due to their flat band-like geometry. The latter possibility is supported by electron microscopy studies which reveal that stress fiber bundles are physically connected to cortical and subcortical actin networks, intermediate filaments, and microtubules (83,84). The larger the stress fiber, the greater the surface area presented to the surrounding cytoskeletal lattice, and hence the more extensive the lateral connections. Similarly, variations of stress fiber location (peripheral versus central) and connectivity (anchored at one end versus both ends) may also give rise to differences in measured elasticity. The experimental approaches described here should help to clarify these regional variations in the future.

The finding that the retraction data are so well described by a viscoelastic cable model is intriguing given recent structural insights into the mechanics of stress fiber contraction. Specifically, when cells containing stress fibers labeled with GFP-tagged MLC and $\alpha$-actinin were treated with contractile agonists, many stress fibers did not appear to contract uniformly along their lengths; instead, myosin activity preferentially concentrated at the stress fiber ends, causing the stress fibers to contract at their peripheries and stretch at their center (85). This would predict either higher contractility or rigidity at the fiber ends compared to its center, and hence that there are significant local variations in its viscoelastic properties. However, we carried out all of our studies in the central region of the cell, far from the distal ends of stress fibers near where they insert into focal adhesions that contain a high density of actin-binding proteins. Thus, our data describe the mechanical behavior of the central portion of the stress fiber, which apparently behaves like a viscoelastic cable that is mechanically homogeneous along its length. Severing stress fibers tagged with internal structural labels at different distances from the focal adhesion along its length should help to clarify these more subtle mechanical responses in the future.

Compromise of a single submicrometer-wide stress fiber located close to the basal cell membrane produces large-scale architectural rearrangements throughout the entire cytoskeleton, changes in overall cell shape, and mechanical restructuring of the ECM when cells are cultured on flexible substrates. This is consistent with the finding that mechanical stresses can be transmitted from the cell apex to the basal membrane of the cell, as well as from the surface membrane to the nucleus, through linked integrins, microfilaments, microtubules, and intermediate filaments that collectively form a single cytoskeletal-integrin-ECM lattice (9,41,86,87). Our work also confirms that cell shape stability requires that this entire cytoskeletal lattice be maintained in a state of isometric tension that, in turn, results from a balance between cytoskeletal tensional forces and the mechanical compliance of the ECM (8–10).

We do not observe large-scale changes in cell and cytoskeletal form when stress fibers are severed in cells adherent to a rigid ECM. Here, cellular remodeling is kept to a minimum, because the rigid ECM is stiff enough to bear the forces transferred from the cut stress fiber without distending or compromising the overall cellular force balance. The fact that actin bundles less than a micrometer away do not

remodel or change their arrangement after irradiation, even on the time scale of minutes, effectively rules out any nonspecific, irradiation-induced change in cellular biochemistry (e.g., local release of calcium) or increase in temperature that might produce local cell contraction. In contrast, when cells are cultured on a more compliant ECM substrate that is already prestressed due to the contractile activity of the adherent cells, disruption of a single stress fiber results in large-scale retraction of the ECM, much like cutting part way through a rope in the midst of a game of tug-of-war would cause the opposing teams to pull away from each other. The retracting ECM pulls the cell adhesions and linked cytoskeleton apart and stretches the entire cell outward until a new force balance is established.

In mechanical terms, the compliance of the ECM controls the degree to which disruption of one stress fiber bundle will influence cell shape in at least two ways. First, a rigid substrate deforms less than a flexible substrate upon absorbing a given amount of traction. Thus, disruption of a stress fiber in a cell cultured on a rigid substrate is expected to produce a smaller change in the strain distribution (distortion) of the substrate compared to a flexible substrate. Cells also actively sense and adapt to the rigidity of the ECM (44,88,89), and greater ECM rigidity increases contractility (44), bolsters focal adhesion size and density (90), and permits greater cell spreading and migration speed (55), implying that focal adhesions in these cells are collectively capable of bearing greater loads.

The ECM rigidity-dependence of the stress fiber contributions to cell shape takes on particular physiological significance when one considers that in living tissues, cells adhere to compliant ECMs and fibrin gels (e.g., during wound healing) whose mechanical properties much more closely resemble a soft gel (Young's moduli ~1–1000 Pa) than a rigid glass surface (28,58,59). Local changes in ECM compliance may therefore provide an important mechanism for effecting rapid changes in cell shape and cytoskeletal structure that may in turn provide a directional cue for migration. This notion is supported by the strong dependence of many cell behaviors on ECM rigidity (55,89,90), and the observation that cell migration may be guided purely by gradients in substrate stiffness, independent of type or density of ECM proteins (75). This force balance manifests itself at the organ/tissue level as well; local changes in cell growth patterns and tissue development can be influenced during embryogenesis by altering the level of cytoskeletal tension within the growing cells that, in turn, alters ECM structure (91). Indeed, during the development of a wide variety of connective tissues, stress fibers increase in prominence during periods of cellular elongation, permitting an oriented deposition of ECM proteins that establishes a scaffold for the architecture of the mature tissue (92). Moreover, in certain tumors, ECM rigidity directly regulates integrin clustering, Rho activity, focal adhesion morphology, stress fiber formation, and ultimately malignant transformation; this provides a subcellular explanation for the clinical correlation between high gross tumor stiffness and poor prognosis (59).

Taken together, these data confirm that isometric tension in the cytoskeleton governs cell shape stability, and that this cellular force balance results from both active actomyosin-based tension generation and passive contributions from the cell's ECM adhesions, as predicted by the tensegrity model of cell mechanics (8). Individual stress fibers located primarily at the cell base therefore stabilize the shape of the whole cell by generating contractile forces and exerting them on their ECM adhesions, and by balancing forces throughout the cell and ECM so as to prestress the entire interconnected cytoskeleton. The use of the laser nanoscissor together with traction force microscopy and photobleaching methods to probe the local viscoelastic properties of the cytoskeletal fibers offers a new tool for spatially-resolved mechanical mapping in living cells.

## SUPPLEMENTARY MATERIAL

An online supplement to this article can be found by visiting BJ Online at http://www.biophysj.org.

We thank D. Weitz and C. Brangwynne for stimulating discussions and N. Wang for his helpful input.

We gratefully acknowledge the support of grants from National Institutes of Health (CA45548 to D.E.I. and postdoctoral fellowship F32-NS048669 to S.K) and from National Science Foundation (DMR-0213805) to the Materials Research and Science Center at Harvard University.

## REFERENCES

1. Chen, C. S., M. Mrksich, S. Huang, G. M. Whitesides, and D. E. Ingber. 1997. Geometric control of cell life and death. *Science*. 276: 1425–1428.
2. Parker, K. K., A. L. Brock, C. Brangwynne, R. J. Mannix, N. Wang, E. Ostuni, N. A. Geisse, J. C. Adams, G. M. Whitesides, and D. E. Ingber. 2002. Directional control of lamellipodia extension by constraining cell shape and orienting cell tractional forces. *FASEB J*. 16:1195–1204.
3. Singhvi, R., A. Kumar, G. P. Lopez, G. N. Stephanopoulos, D. I. C. Wang, G. M. Whitesides, and D. E. Ingber. 1994. Engineering cell-shape and function. *Science*. 264:696–698.
4. McBeath, R., D. M. Pirone, C. M. Nelson, K. Bhadriraju, and C. S. Chen. 2004. Cell shape, cytoskeletal tension, and RhoA regulate stem cell lineage commitment. *Dev. Cell*. 6:483–495.
5. Ridley, A. J., M. A. Schwartz, K. Burridge, R. A. Firtel, M. H. Ginsberg, G. Borisy, J. T. Parsons, and A. R. Horwitz. 2003. Cell migration: integrating signals from front to back. *Science*. 302:1704–1709.
6. Hoh, J. H., and C. A. Schoenenberger. 1994. Surface-morphology and mechanical-properties of MDCK monolayers by atomic force microscopy. *J. Cell Sci.* 107:1105–1114.
7. Litniewski, J., and J. Bereiter-Hahn. 1990. Measurements of cells in culture by scanning acoustic microscopy. *J. Microsc.* 158:95–107.
8. Ingber, D. E. 2003. Tensegrity I. Cell structure and hierarchical systems biology. *J. Cell Sci.* 116:1157–1173.
9. Wang, N., K. Naruse, D. Stamenovic, J. J. Fredberg, S. M. Mijailovich, I. M. Toric-Norrelykke, T. Polte, R. Mannix, and D. E. Ingber. 2001. Mechanical behavior in living cells consistent with the tensegrity model. *Proc. Natl. Acad. Sci. USA*. 98:7765–7770.

10. Wang, N., I. M. Tolic-Norrelykke, J. X. Chen, S. M. Mijailovich, J. P. Butler, J. J. Fredberg, and D. Stamenovic. 2002. Cell prestress. I. Stiffness and prestress are closely associated in adherent contractile cells. *Am. J. Physiol. Cell Physiol.* 282:C606–C616.

11. Stamenovic, D., Z. L. Liang, J. X. Chen, and N. Wang. 2002. Effect of the cytoskeletal prestress on the mechanical impedance of cultured airway smooth muscle cells. *J. Appl. Physiol.* 92:1443–1450.

12. Stamenovic, D., B. Suki, B. Fabry, N. Wang, and J. J. Fredberg. 2004. Rheology of airway smooth muscle cells is associated with cytoskeletal contractile stress. *J. Appl. Physiol.* 96:1600–1605.

13. Heidemann, S. R., and D. Wirtz. 2004. Towards a regional approach to cell mechanics. *Trends Cell Biol.* 14:160–166.

14. Heidemann, S. R., P. Lamoureux, and R. E. Buxbaum. 2000. Opposing views on tensegrity as a structural framework for understanding cell mechanics. *J. Appl. Physiol.* 89:1670–1678.

15. Jenkins, S. 2000. Does tensegrity make the machine work? *Scientist.* 17:26–27.

16. Costa, K. D., W. J. Hucker, and F. C. P. Yin. 2002. Buckling of actin stress fibers: a new wrinkle in the cytoskeletal tapestry. *Cell Motil. Cytoskeleton.* 52:266–274.

17. Kolodney, M. S., and R. B. Wysolmerski. 1992. Isometric contraction by fibroblasts and endothelial cells in tissue culture—a quantitative study. *J. Cell Biol.* 117:73–82.

18. Riveline, D., E. Zamir, N. Q. Balaban, U. S. Schwarz, T. Ishizaki, S. Narumiya, Z. Kam, B. Geiger, and A. D. Bershadsky. 2001. Focal contacts as mechanosensors: externally applied local mechanical force induces growth of focal contacts by an mdia1-dependent and ROCK-independent mechanism. *J. Cell Biol.* 153:1175–1185.

19. Katoh, K., Y. Kano, M. Masuda, H. Onishi, and K. Fujiwara. 1998. Isolation and contraction of the stress fiber. *Mol. Biol. Cell.* 9:1919–1938.

20. Deguchi, S., T. Ohashi, and M. Sato. 2005. Tensile properties of single stress fibers isolated from vascular smooth muscle cells. *J. Biomech.* In press.

21. Gordon, W. E. 1978. Immunofluorescent and ultrastructural studies of sarcomeric units in stress fibers of cultured non-muscle cells. *Exp. Cell Res.* 117:253–260.

22. Sanger, J. W., B. Mittal, and J. M. Sanger. 1984. Analysis of myofibrillar structure and assembly using fluorescently labeled contractile proteins. *J. Cell Biol.* 98:825–833.

23. Kreis, T. E., and W. Birchmeier. 1980. Stress fiber sarcomeres of fibroblasts are contractile. *Cell.* 22:555–561.

24. Anderson, S., L. DiCesare, I. Tan, T. Leung, and N. SundarRaj. 2004. Rho-mediated assembly of stress fibers is differentially regulated in corneal fibroblasts and myofibroblasts. *Exp. Cell Res.* 298:574–583.

25. Chen, B. H., J. T. C. Tzen, A. R. Bresnick, and H. C. Chen. 2002. Roles of Rho-associated kinase and myosin light chain kinase in morphological and migratory defects of focal adhesion kinase-null cells. *J. Biol. Chem.* 277:33857–33863.

26. Katoh, K., Y. Kano, M. Amano, K. Kaibuchi, and K. Fujiwara. 2001. Stress fiber organization regulated by MLCK and Rho-kinase in cultured human fibroblasts. *Am. J. Physiol. Cell Physiol.* 280:C1669–C1679.

27. Sinnett-Smith, J., J. A. Lunn, D. Leopoldt, and E. Rozengurt. 2001. Y-27632, an inhibitor of Rho-associated kinases, prevents tyrosine phosphorylation of focal adhesion kinase and paxillin induced by bombesin: dissociation from tyrosine phosphorylation of p130(cas). *Exp. Cell Res.* 266:292–302.

28. Yeung, T., P. C. Georges, L. A. Flanagan, B. Marg, M. Ortiz, M. Funaki, N. Zahir, W. Y. Ming, V. Weaver, and P. A. Janmey. 2005. Effects of substrate stiffness on cell morphology, cytoskeletal structure, and adhesion. *Cell Motil. Cytoskeleton.* 60:24–34.

29. Gupton, S. L., K. L. Anderson, T. P. Kole, R. S. Fischer, A. Ponti, S. E. Hitchcock-DeGregori, G. Danuser, V. M. Fowler, D. Wirtz, D. Hanein, and others. 2005. Cell migration without a lamellipodium: translation of actin dynamics into cell movement mediated by tropornyosin. *J. Cell Biol.* 168:619–631.

30. Stossel, T. P. 1989. From signal to pseudopod—how cells control cytoplasmic actin assembly. *J. Biol. Chem.* 264:18261–18264.

31. Theriot, J. A., and T. J. Mitchison. 1991. Actin microfilament dynamics in locomoting cells. *Nature.* 352:126–131.

32. Kolega, J., J. W. Janson, and D. L. Taylor. 1991. The role of solation-contraction coupling in regulating stress fiber dynamics in nonmuscle cells. *J. Cell Biol.* 114:993–1003.

33. Strohmeier, R., and J. Bereiter-Hahn. 1984. Control of cell-shape and locomotion by external calcium. *Exp. Cell Res.* 154:412–420.

34. Tseng, Y., K. M. An, and D. Wirtz. 2002. Microheterogeneity controls the rate of gelation of actin filament networks. *J. Biol. Chem.* 277:18143–18150.

35. Bereiter-Hahn, J., M. Luck, T. Miebach, H. K. Stelzer, and M. Voth. 1990. Spreading of trypsinized cells—cytoskeletal dynamics and energy requirements. *J. Cell Sci.* 96:171–188.

36. Mooney, D. J., R. Langer, and D. E. Ingber. 1995. Cytoskeletal filament assembly and the control of cell spreading and function by extracellular-matrix. *J. Cell Sci.* 108:2311–2320.

37. Heisterkamp, A., I. Z. Maxwell, E. Mazur, J. M. Underwood, J. A. Nickerson, S. Kumar, and D. E. Ingber. 2005. Pulse energy dependence of subcellular dissection by femtosecond laser pulses. *Opt. Express.* 13:3690–3696.

38. Shen, N., D. Datta, C. B. Schaffer, P. LeDuc, D. E. Ingber, and E. Mazur. 2005. Ablation of cytoskeletal filaments and mitochondria in cells using a femtosecond laser nanoscissor. *Mech. Chem. Biosyst.* 2:17–25.

39. Koonce, M. P., K. R. Strahs, and M. W. Berns. 1982. Repair of laser-severed stress fibers in myocardial non-muscle cells. *Exp. Cell Res.* 141:375–384.

40. Strahs, K. R., and M. W. Berns. 1979. Laser microirradiation of stress fibers and intermediate filaments in non-muscle cells from cultured rat-heart. *Exp. Cell Res.* 119:31–45.

41. Hu, S., J. Chen, B. Fabry, Y. Numaguchi, A. Gouldstone, D. E. Ingber, J. J. Fredberg, J. P. Butler, and N. Wang. 2003. Intracellular stress tomography reveals stress focusing and structural anisotropy in cytoskeleton of living cells. *Am. J. Physiol. Cell Physiol.* 285:1082–1090.

42. Alenghat, F. J., S. M. Nauli, R. Kolb, J. Zhou, and D. E. Ingber. 2004. Global cytoskeletal control of mechanotransduction in kidney epithelial cells. *Exp. Cell Res.* 301:23–30.

43. Munevar, S., Y. L. Wang, and M. Dembo. 2001. Traction force microscopy of migrating normal and h-ras transformed 3t3 fibroblasts. *Biophys. J.* 80:1744–1757.

44. Polte, T. R., G. S. Eichler, N. Wang, and D. E. Ingber. 2004. Extracellular matrix controls myosin light chain phosphorylation and cell contractility through modulation of cell shape and cytoskeletal prestress. *Am. J. Physiol. Cell Physiol.* 286:C518–C528.

45. Butler, J. P., I. M. Tolic-Norrelykke, B. Fabry, and J. J. Fredberg. 2002. Traction fields, moments, and strain energy that cells exert on their surroundings. *Am. J. Physiol. Cell Physiol.* 282:C595–C605.

46. Landau, L. D., and E. M. Lifshitz. 1986. Theory of Elasticity. Pergammon, Oxford, UK.

47. Botvinick, E. L., V. Venugopalan, J. V. Shah, L. H. Liaw, and M. W. Berns. 2004. Controlled ablation of microtubules using a picosecond laser. *Biophys. J.* 87:4203–4212.

48. Clement, S., B. Hinz, V. Dugina, G. Gabbiani, and C. Chaponnier. 2005. The N-terminal Ac-EEED sequence plays a role in alpha-smooth-muscle actin incorporation into stress fibers. *J. Cell Sci.* 118:1395–1404.

49. McKenna, N. M., and Y. L. Wang. 1986. Possible translocation of actin and alpha-actinin along stress fibers. *Exp. Cell Res.* 167:95–105.

50. Yoon, K. H., M. Yoon, R. D. Moir, S. Khuon, F. W. Flitney, and R. D. Goldman. 2001. Insights into the dynamic properties of keratin intermediate filaments in living epithelial cells. *J. Cell Biol.* 153: 503–516.

51. Osswald, T. A., and G. Menges. 1995. Materials Science of Polymers for Engineers. Hanser/Gardner, Munich, Germany.

52. Canadas, P., V. M. Laurent, C. Oddou, D. Isabey, and S. Wendling. 2002. A cellular tensegrity model to analyse the structural viscoelasticity of the cytoskeleton. *J. Theor. Biol.* 218:155–173.

53. Narumiya, S., T. Ishizaki, and M. Uehata. 2000. Use and properties of ROCK-specific inhibitor Y-27632. *Methods Enzymol.* 325:273–284.

54. Mammoto, A., S. Huang, K. Moore, P. Oh, and D. E. Ingber. 2004. Role of RhoA, mDia, and ROCK in cell shape-dependent control of the skp2-p27(kip1) pathway and the g(1)/s transition. *J. Biol. Chem.* 279: 26323–26330.

55. Peyton, S. R., and A. J. Putnam. 2005. Extracellular matrix rigidity governs smooth muscle cell rigidity in a biphasic fashion. *J. Cell. Physiol.* 204:198–209.

56. Shiu, Y. T., S. Li, W. A. Marganski, S. Usami, M. A. Schwartz, Y. L. Wang, M. Dembo, and S. Chien. 2004. Rho mediates the shear-enhancement of endothelial cell migration and traction force generation. *Biophys. J.* 86:2558–2565.

57. Chen, J., B. Fabry, E. L. Schiffrin, and N. Wang. 2001. Twisting integrin receptors increases endothelin-1 gene expression in endothelial cells. *Am. J. Physiol. Cell Physiol.* 280:C1475–C1484.

58. Engler, A., L. Bacakova, C. Newman, A. Hategan, M. Griffin, and D. Discher. 2004. Substrate compliance versus ligand density in cell on gel responses. *Biophys. J.* 86:617–628.

59. Paszek, M. J., N. Zahir, K. R. Johnson, J. N. Lakins, G. I. Rozengberg, A. Gefen, C. A. Reinhart-King, S. S. Margulies, M. Dembo, D. Boettiger, and others. 2005. Tensional homeostasis and the malignant phenotype. *Cancer Cell.* 8:241–254.

60. Beningo, K. A., M. Dembo, I. Kaverina, J. V. Small, and Y. L. Wang. 2001. Nascent focal adhesions are responsible for the generation of strong propulsive forces in migrating fibroblasts. *J. Cell Biol.* 153: 881–887.

61. Numaguchi, Y., S. Huang, T. R. Polte, G. S. Eichler, N. Wang, and D. E. Ingber. 2003. Caldesmon-dependent switching between capillary endothelial cell growth and apoptosis through modulation of cell shape and contractility. *Angiogenesis.* 6:55–64.

62. Tolic-Norrelykke, I. M., L. Sacconi, G. Thon, and F. S. Pavone. 2004. Positioning and elongation of the fission yeast spindle by microtubule-based pushing. *Curr. Biol.* 14:1181–1186.

63. Khodjakov, A., S. La Terra, and F. Chang. 2004. Laser microsurgery in fission yeast: role of the mitotic spindle midzone in anaphase B. *Curr. Biol.* 14:1330–1340.

64. Watanabe, W., and N. Arakawa. 2004. Femtosecond laser disruption of subcellular organelles in a living cell. *Opt. Express.* 12:4203–4213.

65. Tirlapur, U. K., and K. Konig. 2002. Femtosecond near-infrared laser pulses as a versatile non-invasive tool for intra-tissue nanoprocessing in plants without compromising viability. *Plant J.* 31:365–374.

66. Finer, J. T., R. M. Simmons, and J. A. Spudich. 1994. Single myosin molecule mechanics—piconewton forces and nanometer steps. *Nature.* 368:113–119.

67. Ishii, Y., A. Ishijima, and T. Yanagida. 2001. Single molecule nano-manipulation of biomolecules. *Trends Biotechnol.* 19:211–216.

68. Kojima, H., A. Ishijima, and T. Yanagida. 1994. Direct measurement of stiffness of single actin-filaments with and without tropomyosin by in-vitro nanomanipulation. *Proc. Natl. Acad. Sci. USA.* 91:12962–12966.

69. Liu, X. M., and G. H. Pollack. 2002. Mechanics of f-actin characterized with microfabricated cantilevers. *Biophys. J.* 83:2705–2715.

70. Gardel, M. L., J. H. Shin, F. C. MacKintosh, L. Mahadevan, P. Matsudaira, and D. A. Weitz. 2004. Elastic behavior of cross-linked and bundled actin networks. *Science.* 304:1301–1305.

71. Linke, W. A., and M. C. Leake. 2004. Multiple sources of passive stress relaxation in muscle fibres. *Phys. Med. Biol.* 49:3613–3627.

72. Opitz, C. A., M. Kulke, M. C. Leake, C. Neagoe, H. Hinssen, R. J. Hajjar, and W. A. Linke. 2003. Damped elastic recoil of the titin spring in myofibrils of human myocardium. *Proc. Natl. Acad. Sci. USA.* 100:12688–12693.

73. Cortes, P., M. Mendez, B. L. Riser, C. J. Guerin, A. Rodriguez-Barbero, C. Hassett, and J. Yee. 2000. F-actin fiber distribution in glomerular cells: structural and functional implications. *Kidney Int.* 58:2452–2461.

74. Satcher, R. L., and C. F. Dewey. 1996. Theoretical estimates of mechanical properties of the endothelial cell cytoskeleton. *Biophys. J.* 71:109–118.

75. Lo, C. M., H. B. Wang, M. Dembo, and Y. L. Wang. 2000. Cell movement is guided by the rigidity of the substrate. *Biophys. J.* 79: 144–152.

76. Lele, T. P., J. Pendse, S. Kumar, M. Salanga, J. Karavitis, and D. E. Ingber. 2005. Mechanical forces alter zyxin unbinding kinetics within focal adhesions of living cells. *J. Cell. Physiol.* In press.

77. Maeda, Y., K. Hirano, J. Nishimura, T. Sasaki, and H. Kanaide. 2003. Rho-kinase inhibitor inhibits both myosin phosphorylation-dependent and -independent enhancement of myofilament $Ca^{2+}$ sensitivity in the bovine middle cerebral artery. *Br. J. Pharmacol.* 140:871–880.

78. Nobe, H., K. Nobe, F. Fazal, P. deLanerolle, and R. J. Paul. 2003. Rho kinase mediates serum-induced contraction in fibroblast fibers independent of myosin lc20 phosphorylation. *Am. J. Physiol. Cell Physiol.* 284:C599–C606.

79. Kureishi, Y., S. Kobayashi, M. Amano, K. Kimura, H. Kanaide, T. Nakano, K. Kaibuchi, and M. Ito. 1997. Rho-associated kinase directly induces smooth muscle contraction through myosin light chain phosphorylation. *J. Biol. Chem.* 272:12257–12260.

80. Dudek, S. M., and J. G. Garcia. 2001. Cytoskeletal regulation of pulmonary vascular permeability. *J. Appl. Physiol.* 91:1487–1500.

81. Totsukawa, G., Y. Yamakita, S. Yamashiro, D. J. Hartshorne, Y. Sasaki, and F. Matsumura. 2000. Distinct roles of ROCK (Rho-kinase) and MLCK in spatial regulation of MLC phosphorylation for assembly of stress fibers and focal adhesions in 3T3 fibroblasts. *J. Cell Biol.* 150:797–806.

82. Kaunas, R., P. Nguyen, S. Usami, and S. Chien. 2005. Cooperative effects of Rho and mechanical stretch on stress fiber organization. *Proc. Natl. Acad. Sci. USA.* 102:15895–15900.

83. Marek, L. F., R. O. Kelley, and B. D. Perdue. 1982. Organization of the cytoskeleton in square fibroblasts. *Cell Motil. Cytoskeleton.* 2:115–130.

84. Seifert, G. J., D. Lawson, and G. Wiche. 1992. Immunolocalization of the intermediate filament-associated protein plectin at focal contacts and actin stress fibers. *Eur. J. Cell Biol.* 59:138–147.

85. Peterson, L. J., Z. Rajfur, A. S. Maddox, C. D. Freel, Y. Chen, M. Edlund, C. Otey, and K. Burridge. 2004. Simultaneous stretching and contraction of stress fibers in vivo. *Mol. Biol. Cell.* 15:3497–3508.

86. Maniotis, A. J., C. S. Chen, and D. E. Ingber. 1997. Demonstration of mechanical connections between integrins cytoskeletal filaments, and nucleoplasm that stabilize nuclear structure. *Proc. Natl. Acad. Sci. USA.* 94:849–854.

87. Helmke, B. P., A. B. Rosen, and P. F. Davies. 2003. Mapping mechanical strain of an endogenous cytoskeletal network in living endothelial cells. *Biophys. J.* 84:2691–2699.

88. Choquet, D., D. P. Felsenfeld, and M. P. Sheetz. 1997. Extracellular matrix rigidity causes strengthening of integrin-cytoskeleton linkages. *Cell.* 88:39–48.

89. Engler, A., L. Bacakova, C. Newman, A. Hategan, M. Griffin, and D. Discher. 2004. Substrate compliance versus ligand density in cell on gel responses. *Biophys. J.* 86:617–628.

90. Pelham, R. J., and Y. L. Wang. 1997. Cell locomotion and focal adhesions are regulated by substrate flexibility. *Proc. Natl. Acad. Sci. USA.* 94:13661–13665.

91. Moore, K. A., T. Polte, S. Huang, B. Shi, E. Alsberg, M. E. Sunday, and D. E. Ingber. 2005. Control of basement membrane remodeling and epithelial branching morphogenesis in embryonic lung by Rho and cytoskeletal tension. *Dev. Dyn.* 232:268–281.

92. Hayes, A. J., M. Benjamin, and J. R. Ralphs. 1999. Role of actin stress fibres in the development of the intervertebral disc: cytoskeletal control of extracellular matrix assembly. *Dev. Dyn.* 215:179–189.